# Role of Dry Reforming of Methane for biogenic resource processing

*Alberto Abánades, Bruno Agún, and Elisa Alonso Romero*

*Universidad Politécnica de Madrid, Madrid, Spain, alberto.abanades@upm.es*

**Abstract:**

Dry reforming of methane (DRM) is a very interesting process for greenhouse gases emissions (GHG) control/reduction for its capability to transform two GHG as methane and carbon dioxide into useful energy and vectors. The application of DRM for the integration of biogenic material sources into the circular economy is analysed, identifying its main challenges and barriers. The application of biogas treatment is specifically described for the production of hydrogen, syngas and carbon, including the potential application for clean fuel synthesis. Process simulation is introduced as a valuable input for the techno-economic analysis that will be presented.

The impact of the technological uncertainties for the process, as carbon deposition, heat integration or biogas composition and origin will be discussed. The utilization of liquid metal bubbling reactors, under development in our research group, for the implementation of DRM will be discussed.

**Keywords:**

Dry reforming of methane; liquid metals; biogenic; biogas; carbon; hydrogen; carbon dioxide

# 1. Introduction

The transition towards a sustainable Society implies the change in the way many of our anthropogenic processes are implemented. Humankind needs the shifting from linear processes to circular approaches[1] to minimise waste generation, either from the material, or the energy perspective. The concept of circular bioeconomy has to be developed as well for biogenic resources [2] to further use other than just food production. Material circularity and sector coupling when using biogenic resources is important, affecting aspects as fertilizers, agricultural wastes, technology and energy uses, and the monitoring of the corresponding indicators [3].

Biogas production from several thermal-chemical processes is one of the alternatives for the biowaste management via its valorization as energy. Biogas composition is mainly characterised by a variable $CH_4/CO_2$ ratio dependant on the transformation process and the feedstock. Anaerobic digestion is the main industrial source of biogas. Given the heterogeneous nature of organic matter and reaction routes of the anaerobic digestion process, the $CH_4/CO_2$ can vary significantly. Typically, biogas is composed of approximately 55–75% biomethane ($CH_4$), 25– 45% carbon dioxide ($CO_2$), and trace amounts of other gaseous compounds.

Dry Reforming of Methane (DRM) represents one of the most promising routes for syngas production, enabling the simultaneous valorization of two major greenhouse gases, $CH_4$ and $CO_2$, in an endothermic reaction that typically requires temperatures above 1073–1173 K to achieve adequate conversion and process performance. Operating at those temperatures is a challenge. In most of the cases, catalysts are used to allow reduce process temperatures. That is a solution than certainly is very convenient, but now is facing with material and circular issues, as most of the catalysts are considered critical raw materials and their recovery/ regeneration usually implies $CO_2$ release, especially when developing reactions involving coke formation [4].

We are developing non-catalytic methane splitting by gas bubbling into a liquid metal bath. One of the activities for the future of our liquid metal technology is the application of this know-how to other processes with the potential production of coke and high temperature operation. The selection of an efficient heat transfer fluid (HTF) is a critical aspect in the design and operation of DRM reactors, as it determines the system's ability to maintain these high temperatures in a stable, safe, and economically viable manner. Liquid metals are a suitable reaction environment to process such gaseous substances. Furthermore, rapid catalyst deactivation due to coke formation poses a significant barrier to industrial deployment[5], and operation at high temperature allows to avoid the extensive use of catalysts, improving one of the aspects more relevant for the environmental and material impact of $CO_2$ processing.

# 2. Dry Reforming of Methane

## 2.1. Chemical reactions

The equilibrium composition is governed by three independent reactions that generates the relevant chemistry of the $CH_4$–$CO_2$ system at high temperature. The primary DRM reaction (R1) produces syngas from equimolar feeds:

$$CH_4 + CO_2 \rightarrow 2\,CO + 2\,H_2 \qquad \Delta H°_{298} = +247 \text{ kJ mol}^{-1} \qquad \text{(R1)}$$

At temperatures above approximately 900 °C, methane pyrolysis (R2) becomes significant and provides an additional source of $H_2$ together with solid carbon:

$$CH_4 \rightarrow C(s) + 2\,H_2 \qquad \Delta H°_{298} = +74.9 \text{ kJ mol}^{-1} \qquad \text{(R2)}$$

The reverse water-gas shift reaction (R3) couples $H_2$ and $CO_2$ consumption and governs $H_2O$ formation:

$$CO_2 + H_2 \rightarrow CO + H_2O \qquad \Delta H°_{298} = +41.4 \text{ kJ mol}^{-1} \qquad \text{(R3)}$$

These three reactions form a complete independent set for the six-species system ($CH_4$, $CO_2$, CO, $H_2$, $H_2O$, C(s)}, as can be verified by rank analysis of the stoichiometric matrix [6], [7]. The Boudouard reaction ($2CO \rightleftharpoons C + CO_2$) and CO hydrogenation are linearly dependent combinations of R1–R3 and are therefore implicitly accounted for.

## 2.2. Equilibrium model

The equilibrium state was determined by direct minimisation of the total Gibbs free energy of the system, following the reaction-extent formulation of [8] as applied to the DRM system by [9]. Three independent reaction extents $\xi_1$, $\xi_2$, $\xi_3$ (corresponding to R1, R2 and R3, respectively) uniquely determine the molar amounts of all species through the atom-balance constraints:

$$n_{CH_4} = n°_{CH_4} - \xi_1 - \xi_2$$
$$nCO_2 = n°_{CO_2} - \xi_1 - \xi_3$$
$$n_{CO} = 2\xi_1 + \xi_3$$
$$n_{H_2} = 2\xi_1 + 2\xi_2 - \xi_3$$
$$n_{H_2O} = \xi_3$$
$$n_{C(s)} = \xi_2$$

where n° denotes the initial molar amount of each species. The total Gibbs free energy to be minimised is:

$$G_{tot} = n_{C(s)} \cdot G°_C + \Sigma_i\, n_i\, [G°_i(T) + RT\, ln(n_i / n_{gas})] \qquad (1)$$

where the summation runs over the five gas-phase species, $n_{gas} = \Sigma n_i$ is the total number of moles of gas (the mole fraction serves as the fugacity at atmospheric pressure), $R = 8.314 \cdot 10^{-3}$ kJ/mol·K and $G°_i(T) = H°_i(T) - T \cdot S°_i(T)$ is the standard molar Gibbs energy computed from NIST-JANAF Shomate polynomials (see Annex). The solid carbon phase contributes only its standard Gibbs energy, as its activity is unity.

Minimisation was performed numerically using the Nelder–Mead simplex algorithm over the three-dimensional space of reaction extents. To ensure convergence to the global minimum — critical in systems with multiple local minima — a structured grid of 10 × 10 starting points was generated by systematically sampling the feasible space ($\xi_1 \in [0, \min(n°_{CH_4}, n°_{CO_2})]$, $\xi_2 \in [0, n°_{CH_4} - n°_{CO_2}]$, $\xi_3 \in [-0.3, 0.3]\, n°_{CO_2}$). The solution with the lowest $G_{tot}$ satisfying the non-negativity constraint on all species ($n_i \geq 0$) was retained. Convergence tolerances were set to 10–11 on the variable space and 10–12 on the function value, ensuring thermodynamically self-consistent results.

Figure 1 presents the model predictions for operating conditions of 1 atm pressure and a $CH_4/CO_2$ molar ratio of 2, in order to compare the results with those reported in Figure 1a of [9]. The data from that figure have been incorporated into the present plot to enable direct comparison with the outcomes of our model. Overall, the agreement is good, although slightly higher solid carbon production is observed in the results reported by [9]. This difference is likely due to the treatment of the various solid carbon phases, since in the present work only a single solid phase has been considered.

Following, different reactants molar ratios are introduced in the thermodynamic model in order to know its effect in the equilibrium composition, and depicted in Figure 2 for $CH_4/CO_2$ ratios from 0.5 to 3.

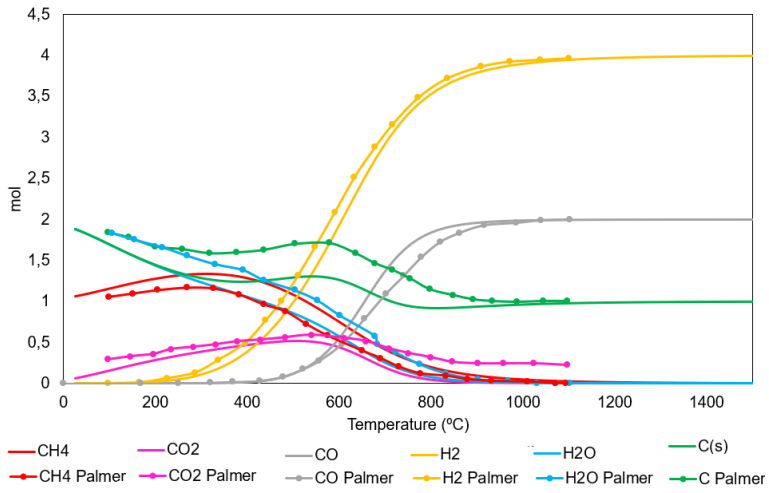


***Figure 1.*** *Thermodynamic equilibrium of dry reforming compounds compared to the results obtained by [7]*

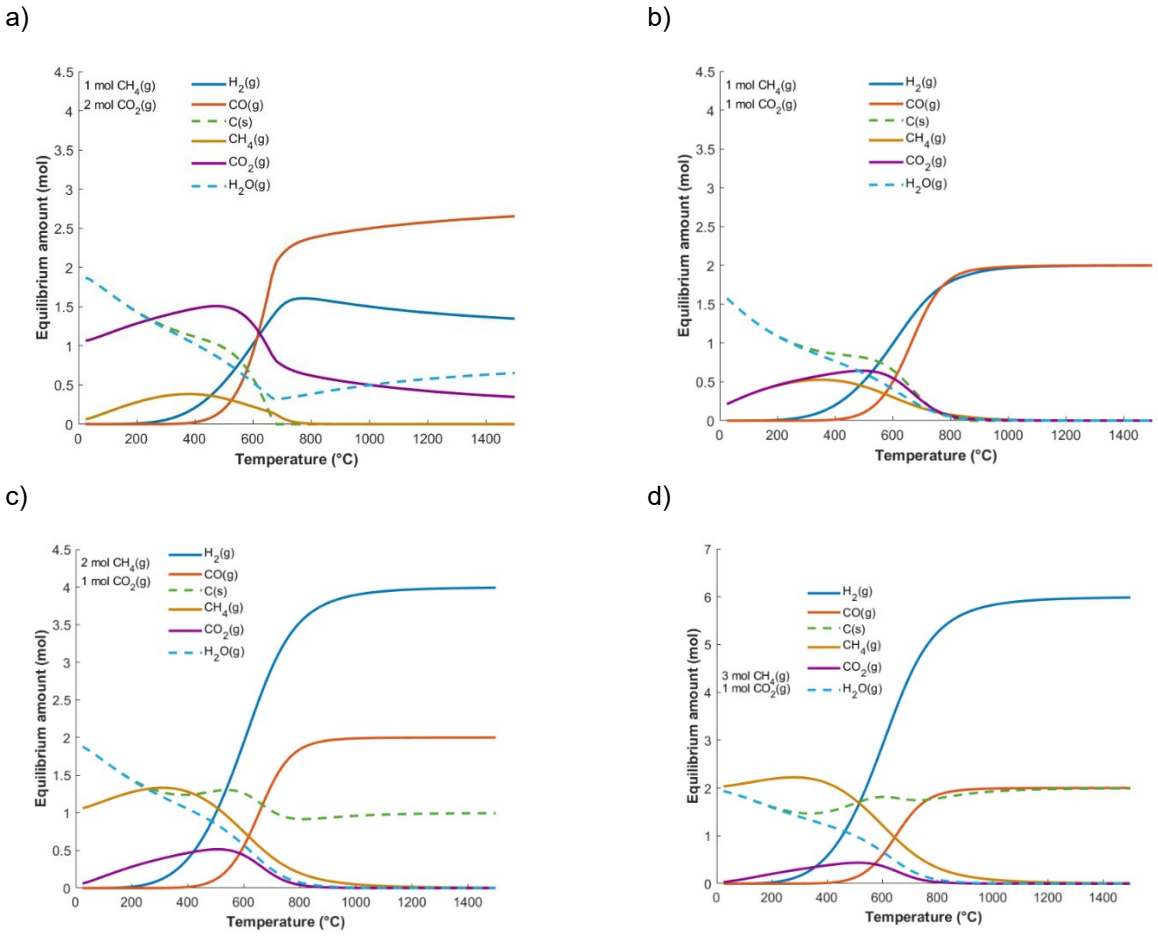


***Figure 2.*** *Thermodynamic equilibrium of dry reforming for different $CH_4/CO_2$ molar ratio. a) molar ratio=1/2, b) molar ratio=1/1, c) molar ratio=2/1, d) molar ration =3/1.*

# 3. Engineering process

To complement the equilibrium analysis, kinetic simulations were performed in DWSIM version 9.0.2, an open-source chemical engineering simulator that offers easy access, a powerful thermodynamic package, and an interactive graphical interface for process analysis, using a user-defined Plug-Flow Reactor (PFR) with custom Python scripts. The model includes two material streams (feed stream and syngas product) and an operation

unit (a plug flow reactor). In summary, $CH_4$ and $CO_2$ enter as a hot gas mixture into the reactor, where DRM conversion takes place following a Phyton script with our previous kinetic model and producing syngas. The model calculates the conversion, selectivity, and concentration profile along the reactor length by integrating the rate equations.

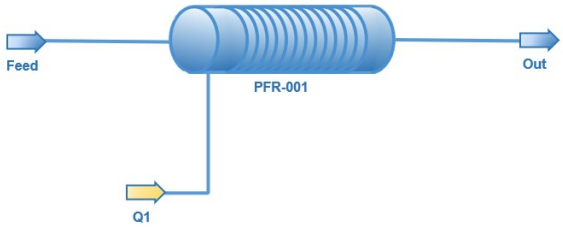


***Figure 3.*** *DWSIM Flowsheet with a simple Plug-Flow reactor scheme.*

The assumed design conditions and parameters are as follows as recommended by Luyben et al [8].

- The reactor temperature is fixed at 1273 K (isothermal).
- The flow rate is 0.00925 $mol \cdot s^{-1}$; and may be adjusted if deemed necessary in specific scenarios.
- The $CH_4/CO_2$ flow rate is 1; the $CO_2$ concentration influences a small fraction of the water formed due to the RWGS (Reverse Water Gas Shift) reaction.
- Heaters, compressors, and water-cooled gas heat exchangers are not included in the process configuration, they could include in a future simulation more realistic.
- This setup is used to determine the reactor effluent conditions.

Besides, to simplify the model, the following assumptions are made:

- $CH_4$ and $CO_2$ are considered pure gases, free of any impurities.
- the RWGS reaction is assumed to be the only side reaction occurring during reforming
- Since the catalyst is the liquid metal, we considered the entire reactor volume as the catalyst. However, in the heterogeneous catalyst reactor, we often have a catalyst bed. We considered the reactor as a filled tube with the liquid metal. Therefore, the catalyst volume is the same as the reactor volume, assuming the void fraction 1.
- Three effective parameters are considered for the inlet: the liquid-metal surface temperature ($T_{wall}$), the flow rate with the methane-to–carbon dioxide ratio ($CH_4/CO_2$), and the reactor pressure. It is assumed that the feed contains no hydrogen, carbon monoxide, or water [10].

We have included in our reactor a kinetic model based on the reactions and kinetic parameters shown on Table 2 and Table 3, for the reaction scheme of Figure 4.

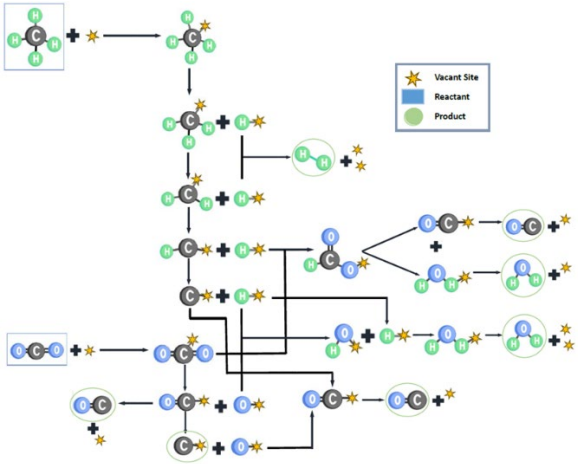


***Figure 4.*** *scheme of the employed elementary reactions. When the specie is joint to a vacant site, it is an adsorbed species*

***Table 1:*** *Detailed Kinetic Model Mechanism for DRM, RWGS and Gasification Reactions.*

| N. | Elementary reaction | Const. | Reaction pathway |
|---|---|---|---|
| ➢ **Adsorption:** | | | |
| 1 | $CH_4 + * \rightarrow CH_4*$ | $K_1$ | Molecular $CH_4$ adsorption (weak) |
| 2 | $CO_2 + * \rightleftharpoons CO_2*$ | $K_2$ | Molecular $CO_2$ adsorption |
| 3 | $H_2 + 2* \rightleftharpoons H* + H*$ | $K_3$ | Dissociative $H_2$ adsorption |
| ➢ **Surface reactions:** | | | |
| 4 | $CH_4* + * \rightleftharpoons CH_3* + H*$ | $k_4$, $k_{-4}$ | First C-H bond cleavage, $CH_4$ dissociation on the metal **(RDS for DRM)**. |
| 5 | $CH_3* + * \rightleftharpoons CH_2* + H*$ | $K_5$ | Fast equilibrium |
| 6 | $CH_2* + * \rightleftharpoons CH* + H*$ | $K_6$ | Fast equilibrium |
| 7 | $CH* + * \rightleftharpoons C* + H*$ | $K_7$ | Fast equilibrium |
| 8 | $CO_2* + * \rightleftharpoons CO* + O*$ | $K_8$ | $CO_2$ dissociation on the metal, activation of $CO_2$ (fast) |
| 9 | $CO* + * \rightarrow C* + O*$ | $K_9$ | CO dissociative equilibrium |
| 10 | $O* + C* \rightleftharpoons CO* + *$ | $K_{10}$ | Carbon gasification by oxygen (fast) |
| 11 | $CO_2* + H* \rightleftharpoons HCOO* + *$ | $k_{11}$, $k_{-11}$ | Formate formation, adsorbed hydrogen species react with $CO_2$ **(RDS for RWGS)** |
| 12 | $HCOO* + H* \rightleftharpoons CO* + H_2O*$ | $K_{12}$ | Formation of $H_2O$ and CO (Fast decomposition) |
| 13 | $O* + H* \rightleftharpoons OH* + *$ | $K_{13}$ | Oxidation of H* (Fast equilibrium) |
| 14 | $OH* + H* \rightleftharpoons H_2O* + *$ | $K_{14}$ | Dissociative pathway for RWGS (Fast equilibrium) |
| 15 | $C* + H_2O* \rightleftharpoons CH* + OH*$ | $K_{15}$ | $H_2O$ inhabitation of carbon formation (Steam gasification equilibrium) |
| 16 | $C* + OH* \rightleftharpoons CH* + O*$ | $K_{16}$ | Hydroxylacion gasification |
| 17 | $CO* + H* \rightleftharpoons HCO* + *$ | $K_{17}$ | Formyl formation |
| 18 | $C* + OH* \rightleftharpoons HCO* + *$ | $K_{18}$ | Alternative formyl pathway |
| 19 | $2CO* \rightarrow CO_2* + C*$ | $K_{19}$ | Boudouard equilibrium |
| 20 | $CO_2* + C* \rightarrow 2CO* + *$ | $K_{20}$ | $CO_2$ gasification equilibrium |
| ➢ **Desorption:** | | | |
| 21 | $CO* \rightleftharpoons CO + *$ | $K_{21}$ | CO desorption (fast) |
| 22 | $H* + H* \rightleftharpoons H_{2(g)} + 2*$ | $K_{22}$ | $H_2$ desorption (fast) |
| 23 | $H_2O* \rightleftharpoons H_2O_{(g)} + *$ | $K_{23}$ | $H_2O$ desorption (fast) |

Reactor performed under isothermal operation at 1215 K, the PFR achieved methane conversions of 70-85 % and a carbon dioxide conversion ranged from 85-100 %, consistently higher than methane conversion due to simultaneous consumption via both DRM and RWGS pathways and with slight variations attributable to numerical solver tolerances. The CO selectivity exceeded 80 % across all conditions, with $H_2$/CO ratios lower than unity, indicating significant RWGS contribution that consumes $H_2$ while producing additional CO. Water production via RWGS reached maximum yields of 10% of total products, with complete consumption predicted in downstream water-gas shift units.

As expected from the equilibrium model, the kinetic model verify that significant carbon formation is also produced with $CH_4/CO_2$ ratios higher than 2, as methane provide a carbon excess respect the equilibrium conversion of CO. Consequently, low $CH_4/CO_2$ ratios, may also lead to the production of significant amounts of water in excess. That is important to evaluate operation procedures adapted to the characteristics of the input gases to the process, as well as to allow to run the process with a flexibility that could allow to produce different products. For instance, depending on the $CH_4/CO_2$ pre-adjustment and the market needs produce more or less carbon, or syngas.

***Table 2:*** *Kinetic parameters (reaction rate, absorption, and equilibrium constants) assumed for Sn Liquid metal catalyst in mol $kg^{-1}s^{-1}$ [11]*

| Parameter | Value | Parameter | Value |
|---|---|---|---|
| **DRM** | | **RWGS** | |
| **Reaction rate constants (Arrhenius' law)** | | | |
| $k_4 = k_{DRM}$ | $1.29 \cdot 10^{6} \exp\left(-\frac{1020635}{R\,T}\right)$ | $k_{11} = k_{RWGS}$ | $0.35 \cdot 10^{6} \exp\left(-\frac{81030}{R\,T}\right)$ |
| **Absorption constants (Van't Hoff Form)** | | | |
| $K_1 = K_{CH4}$ | $2.0 \cdot 10^{-6} \exp\left(+\frac{40684}{R\,T}\right)$ | $K_1 = K_{CH4}$ | $2.00 \cdot 10^{-6} \exp\left(+\frac{40684}{R\,T}\right)$ |
| $K_2 = K_{CO2}$ | $7.4 \cdot 10^{-8} \exp\left(+\frac{4900}{R\,T}\right)$ | $K_2 = K_{CO2}$ | $7.4 \cdot 10^{-8} \exp\left(+\frac{4900}{R\,T}\right)$ |
| $K_3 = K_{H2}$ | $4.1 \cdot 10^{-7} \exp\left(-\frac{133210}{R\,T}\right)$ | $K_3 = K_{H2}$ | $4.1 \cdot 10^{-7} \exp\left(-\frac{133210}{R\,T}\right)$ |
| $K_{-21} = K_{CO}$ | $8.1\,10^{-8} \exp\left(+\frac{80395}{R\,T}\right)$ | $K_{-21} = K_{CO}$ | $8.1\,10^{-8} \exp\left(+\frac{80395}{R\,T}\right)$ |
| $K_{-23} = K_{H2O}$ | $8.0 \cdot 10^{-10} \exp\left(+\frac{-57770}{R\,T}\right)$ | $K_{-23} = K_{H2O}$ | $8.0 \cdot 10^{-10} \exp\left(+\frac{-57770}{R\,T}\right)$ |
| **Equilibrium constants** | | | |
| $K_4 = K_{DRM}$ | $2.82 \cdot 10^{16} \exp\left(-\frac{131500}{R\,T}\right)$ | $K_{11} = K_{RWGS}$ | $56.4971 \exp\left(-\frac{36580}{R\,T}\right)$ |

In Figure 5 the increase in conversion with temperature follows the endothermic nature of DRM, while the $H_2$/CO ratio remaining below 1 confirms the persistent influence of the RWGS side reaction across the temperature range. The predicted conversions (75-95 % at 1215 K[12] ) align well with our simulation for Sn-based liquid metal with no catalysts (30-50 % at comparable conditions). The model overpredicted $CO_2$ conversion compared to literature values. Additionally, the model does not account for catalyst degradation or carbon deposition, which are known challenges in DRM but are mitigated in liquid metal systems.

The simulation results provide several key insights for liquid metal DRM reactor design:

- Optimal Temperature: 1150-1250 K balances reasonable conversion (60-85 %) with manageable thermal loads.
- Catalyst Loading: 200-300 kg/m³ offers the best trade-off between conversion and reactor cost.
- Feed Composition: $CO_2/CH_4$ ratios of 1.0-1.2 maximize conversion while minimizing carbon risk.
- The kinetic model demonstrates excellent predictive capability within the calibrated range (1100-1300 K, 1-10 bar). However, these conditions still require validation, particularly for pressure effects on adsorption constants.

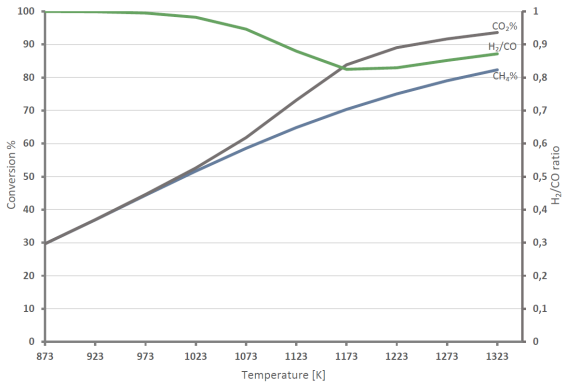


**Figure 5 .** *Effect of temperature on DRM performance using the Sn-based liquid metal catalyst model and kinetic parameters from table 2. The plot shows $CH_4$ and $CO_2$ conversion and $H_2$/CO product ratio, as a function of temperature for an isothermal PFR with an equimolar feed at atmospheric pressure.*

# 4. Application to clean fuel production

Regarding the production of clean fuels and renewable gases. Biogas can be directly used as clean fuel as it is produced from biogenic sources, or being processed to produce valuable products, for instance, methanol, that is easier to transport and with higher energy density, being a promising candidate as clean sustainable shipping or aviation fuel. Typically, biogas is composed of approximately 55– 75% biomethane ($CH_4$), 25– 45% carbon dioxide ($CO_2$), and trace amounts of other gaseous compounds[10]

The dry reforming has the flexibility to be applied to several types of $CH_4/CO_2$ ratios, with higher $H_2$ generation potential, the higher that ratio. Syngas produced by the dry reforming of the biogas stream contains a variable amount of CO and H2. Those gases mat be considered the bricks for the production of any type of synthetic fuel, as methanol, ethanol or others. For the synthesis of methanol, containing a high hydrogenation, the amount of $H_2$ production may be maximised, typically with a water-shift reaction that reduced the water that is added into hydrogen, following the scheme on Figure 6.

Depending on the type of biogas, characterized by that $CH_4/CO_2$ ratio, certain amount of methanol will be produced. A mass balance assuming the parameters in Table 3, we achieve the production of 38 kg/h of $CH_3OH$, with a neutral balance of $CO_2$ (as the result of the process produced as well the original 60 kg/h of $CO_x$). Therefore, we consider that lower $CO_2$ emission could be achieved with hybridization with other $H_2$ production processes as electrolysis or methane splitting.

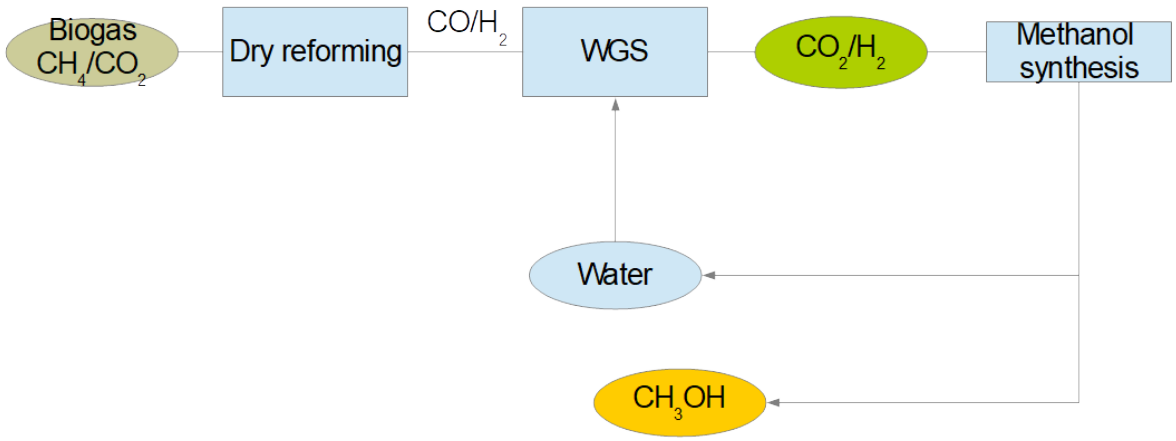


**Figure 6.** *Synthesis of methanol from dry reforming of biogas.*

***Table 3.*** *Summary of hypothesis and operational data for the biogas processing scheme.*

| **Biogas** | | Comment |
|---|---|---|
| Composition | 60% $CO_2$; 40% $CH_4$ | Reference composition compatible with different substrates and processes. |
| Mass flow | 100 kg/h | Typical amount corresponding to TRL7 |
| **Processes, conversion rates** | | |
| Dry reforming | 80% | It is assumed that it is not achieved a complete conversion of the reactants into products. |
| Water-Gas-Shift | 85% | |
| Methanol synthesis | 90% | |

***Table 4.*** *Economic data for the estimation of biogas processing scheme.*

| **CAPEX** | Value | Reference |
|---|---|---|
| Biogas upgrading | 0.45 €/kg | [13] |

| | | |
|---|---|---|
| Methanol Synthesis | 0.49 €/W | [14] |
| Dry reforming | 1.2 €/W | [15] |
| WGS reactor | 0.24 €/ | [15] |
| Heat exchangers | 25 €/W/K | |
| Auxiliary systems | CAPEX reactors | |
| **OPEX** | 3% CAPEX | |
| **Biogas cost** | 0.25 €/kg | |
| **Interest rate (r)** | 3% | |
| **Time (t)** | 15 years | |
| **Capacity factor** | 83% (7200 h) | |

We have evaluated the cost of the production of methanol with the data on Table 4 on equation (2), that returns the levelized cost of methanol (LCOMe) from the capital expenditure of the reactors at the three steps of the process (dry reforming, water-gas shift and methanol synthesis), and the operational expenditure (OPEX), considering the cost of the biogas an independent variable that will impact the total cost.

$$LCOMe = \frac{CAPEX + \sum_{t=1}^{n} \frac{OPEX + C_{biogas}}{(1+r)^t}}{\frac{P_{CH3OH}}{(1+r)^t}} \quad (2)$$

For a facility processing 100 kg/h of biogas, producing 38 kg/h, we evaluate the production cost of the order of 1.8 €/kg, what is double of the current price of methanol in the market.

# 5. Conclusion

Dry reforming of methane is a promising process to extend the utilization of biogas to other sectors and produce hydrogen and carbon, and synthesis for the energy and materials sector. One of the technological challenges for the process is the coke accumulation that is formed within the transition between the methane splitting and the subsequent carbon gasification. To avoid such coke formation, that affect as well catalyst deactivation, we are analysing the utilization of liquid metal media, in particular liquid tin, to carry on the process. Apart of the kinetic analysis, that needs the evaluation of accurate kinetic parameters in liquid metal environment, another problem is the economics of the process, especially in the context of its application to clean fuels. We have evaluated the production route for methanol from syngas produced by the DRM processes, showing that some improvements are needed to compete with fossil-derived methanol.

# Appendix A

Standard enthalpies and entropies were calculated from NIST Shomate polynomials for all six species ($CH_4$, $CO_2$, CO, $H_2$, $H_2O$(g), C(graphite)). For each species, two temperature ranges are used (Table 1), with range boundaries at 1000–1700 K depending on the species. The Shomate expressions are:

$$H°(T) - H°(298\ K) = At + Bt^2/2 + Ct^3/3 + Dt^4/4 - E/t + F \quad [\text{kJ mol}^{-1}] \quad (2)$$

$$S°(T) = A\ ln(t) + Bt + Ct^2/2 + Dt^3/3 - E/(2t^2) + G \quad [\text{J mol}^{-1}\ \text{K}^{-1}] \quad (3)$$

where $t = T$(K)/1000. For C(graphite), the reference enthalpy offset $H°$(298 K) = 7.3301 kJ/mol (low-temperature range) obtained from the Shomate polynomial at 298 K was subtracted to enforce the standard-state convention $H°_f$(C, graphite, 298 K) = 0 [5]. Continuity of $H°(T)$ and $S°(T)$ across range boundaries was verified analytically. Model validation was performed by computing $G°(T)$ for each species at 1000 °C and checking that the standard Gibbs energy change of reaction R1 satisfies $\Delta G°_{DRM} \approx -102$ kJ/mol, in agreement with published values [1,4].

***Table 5.*** *Temperature ranges for NIST Shomate polynomials used in this work.*

| Species | Low − T range (K) | High − T range (K) |
|---|---|---|
| $CH_4$ | 298-1300 | 1300-6000 |
| $CO_2$ | 298-1200 | 1200-6000 |
| CO | 298-1300 | 1300-6000 |
| $H_2$ | 298-1000 | 1000-6000 |
| $H_2O$(g) | 500-1700 | 1700-6000 |
| C (graf.) | 298-1200 | 1200-6000 |

# References


[1] M. Yang *et al.*, “Circular economy strategies for combating climate change and other environmental issues,” *Environ. Chem. Lett.*, vol. 21, no. 1, pp. 55–80, 2023, doi: 10.1007/s10311-022-01499-6.

[2] W. Jander, J. Günther, and A. Prochnow, “What is this thing called circular bioeconomy? Integrating the concepts of circular agri-food and industrial systems,” *J. Clean. Prod.*, vol. 530, p. 146872, 2025, doi: https://doi.org/10.1016/j.jclepro.2025.146872.

[3] G. Moraga *et al.*, “Circular economy indicators: What do they measure?,” *Resour. Conserv. Recycl.*, vol. 146, pp. 452–461, 2019, doi: https://doi.org/10.1016/j.resconrec.2019.03.045.

[4] R. Y. Chein, Y. C. Chen, C. T. Yu, and J. N. Chung, “Thermodynamic analysis of dry reforming of CH4 with CO2 at high pressures,” *J. Nat. Gas Sci. Eng.*, vol. 26, pp. 617–629, 2015, doi: https://doi.org/10.1016/j.jngse.2015.07.001.

[5] M. K. Nikoo and N. A. S. Amin, “Thermodynamic analysis of carbon dioxide reforming of methane in view of solid carbon formation,” *Fuel Processing Technology*, vol. 92, no. 3, pp. 678–691, 2011, doi: https://doi.org/10.1016/j.fuproc.2010.11.027.

[6] J. M. Smith, H. C. Van Ness, and M. Abbott, *Introduction to Chemical Engineering Thermodynamics*. in CHEMICAL ENGINEERING SERIES. McGraw-Hill Education, 2005.

[7] C. Palmer, D. C. Upham, S. Smart, M. J. Gordon, H. Metiu, and E. W. McFarland, “Dry reforming of methane catalysed by molten metal alloys,” *Nat. Catal.*, vol. 3, no. 1, pp. 83–89, 2020, doi: 10.1038/s41929-019-0416-2.

[8] W. L. Luyben, “Design and Control of the Dry Methane Reforming Process,” *Ind. Eng. Chem. Res.*, vol. 53, no. 37, pp. 14423–14439, Sep. 2014, doi: 10.1021/ie5023942.

[9] A. Behroozsarand and A. N. Pour, “Modeling of microreactor for methane dry reforming: Comparison of Langmuir–Hinshelwood kinetic and microkinetic models,” *J. Nat. Gas Sci. Eng.*, vol. 20, pp. 99–108, 2014, doi: https://doi.org/10.1016/j.jngse.2014.06.011.

[10] D. Deublein and A. Steinhauser, *Biogas from Waste and Renewable Resources. An Introduction*. WILEY-VCH Verlag GmbH & Co. KGaA, 2008.

[11] Y. Benguerba, L. Dehimi, M. Virginie, C. Dumas, and B. Ernst, "Numerical investigation of the optimal operative conditions for the dry reforming reaction in a fixed-bed reactor: role of the carbon deposition and gasification reactions," *Reaction Kinetics, Mechanisms and Catalysis*, vol. 115, no. 2, pp. 483–497, 2015, doi: 10.1007/s11144-015-0849-9.

[12] J. Silva, J. C. Gonçalves, C. Rocha, J. Vilaça, and L. M. Madeira, "Biomethane production from biogas obtained in wastewater treatment plants: Process optimization and economic analysis," *Renewable Energy*, vol. 220, p. 119469, 2024, doi: https://doi.org/10.1016/j.renene.2023.119469.

[13] E. Moioli, A. Wötzel, and T. Schildhauer, "Feasibility assessment of small-scale methanol production via power-to-X," *Journal of Cleaner Production*, vol. 359, p. 132071, 2022, doi: https://doi.org/10.1016/j.jclepro.2022.132071.

[14] E. Villa-Ávila, P. Arévalo, M. Tostado-Véliz, and F. Jurado, "Electrolyzers for H 2 Production," in *Towards Green Hydrogen Generation*, 2024, pp. 359–406. doi: https://doi.org/10.1002/9781394234110.ch11.